Surface Effect on Young's Modulus of Sub-Two-Nanometer Gold [111] Nanocontacts

Jiaqi Zhang,[1] Masahiko Tomitori,[1] Toyoko Arai,[2] and Yoshifumi Oshima[1,*]
[1]School of Materials Science, Japan Advanced Institute of Science and Technology, Nomi, Ishikawa 923-1292, Japan
[2]Institute of Science and Engineering, Kanazawa University, Kanazawa, Ishikawa 920-1192, Japan

(Received 29 July 2021; accepted 11 March 2022; published 5 April 2022)

The surface bond nature of face centered cubic metals has been controversial between hardening and softening theoretically because of the lack of precise measurement. Here, we precisely measured the size dependence of Young's modulus of gold [111] nanocontacts with a clean surface by our *in situ* TEM-frequency modulation force sensing method in ultrahigh vacuum at room temperature. Young's modulus gradually decreased from ca. 80 to 30 GPa, as the nanocontact width decreased below 2 nm, which could be explained by surface softening; Young's modulus of the outermost atomic layer was estimated to be approximately 22 GPa, while that of the other part was almost the same with the bulk.

DOI: 10.1103/PhysRevLett.128.146101

When the size of a metal material is reduced to a few nanometers, the surface effect becomes significant, leading to different physical and chemical properties from their bulk counterparts [1–3]; for example, the emergence of quantized conductance [4] and the formation of single Au and Pt nanotubes [5–7]. Surface effects have also emerged as the change of the mechanical properties of atomic scale materials [8–10], which have attracted considerable interest not only in basic research but also in applications for nanoelectromechanical systems (NEMSs) such as force sensors and stretchable devices [11–15]. Among them, Young's modulus is one of the fundamental elastic responses, because it determines the resonant frequency of elastic waves propagating in the nanomaterial, which is a key issue in designing NEMS.

Theoretical investigations suggested that Young's modulus was determined by competition between softening caused by a reduction in the coordination number of surface atoms, and hardening caused by the redistribution of electrons of the surface atoms [8,16–18]. Wang *et al.* predicted that Young's modulus of Au nanowires (NWs) increased with the reduction of the diameter of Au nanowires owing to the surface tension by the DFT calculations [19]. Also, by molecular dynamic simulations, Liu *et al.* showed the similar tendency for Au [100], [110], and [111] NWs [20]. On the other hand, Zhang *et al.* [9] and Wang *et al.* [21] showed that Young's modulus decreased with a decrease of diameter in simulation, which was explained in terms of the surface elasticity. In addition, considering a Au NW of a few nm in diameter was almost single crystalline and defect-free [22,23], Young's modulus was suggested to depend not only on sample size but also on its orientation. However, a consensus has not been reached [24,25].

Experimentally, the elastic properties have been investigated for semiconducting and metallic NWs [26–30]. Young's modulus of GaAs or Si NWs have been reported to increase with reducing diameter when an amorphous or oxidation layer was formed on the surface [31,32], while one of the clean Si NWs was reported to show the opposite size dependence [33]. In addition, Chen *et al.* estimated Young's modulus for Al_2O_3 films of 2 nm to several nm in thickness which were coated on the GaAs NWs [34]. These results suggested that the material adsorbed on the NW has an influence on its elastic property [35]. On the other hand, for Au NWs, Young's modulus did not show the size dependence with a diameter in the range of 50–200 nm [36]. The surface to volume ratio seems to be too small to detect the surface effect in such range. Therefore, elucidation of the surface effect on the mechanical properties of metal NWs remains as a major challenge.

In this Letter, we measured the evolution of structure and stiffness of the Au nanocontacts (NCs) with axis along the ⟨111⟩ direction (Au ⟨111⟩ NC) in the stretching process by our developed transmission electron microscope (TEM) holder equipped with a quartz length-extension resonator (LER) [37–39]. We found that a (111) layer was introduced at the narrowest constriction every ca. 0.24 nm elongation, which made stepwise change in conductance. From the stiffness difference before and after the introduction, Young's modulus was estimated for the introduced (111) layer. We found that Young's modulus gradually decreased from ca. 80 to 30 GPa as the nanocontact diameter decreased below 2 nm. Such a reduction was explained by surface softening.

Figure 1(a) shows the schematic of the experimental setup with the Au NC in the TEM holder of an ultrahigh vacuum TEM (UHV-TEM, JEM-2000VF, 200 kV) operating under conditions of 10^{-7} Pa. The Au NC was fabricated by making a contact between two sharpened Au wires (99.99% purity, Nilaco), one fixed to the edge of the LER (3EXW-1073, STATEK) and the other fixed to a counterelectrode. The position of the LER-side Au wire

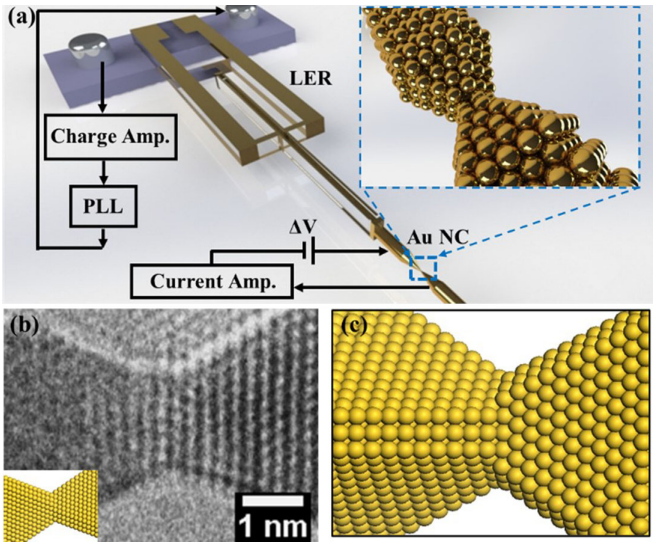

FIG. 1. (a) Schematic illustration of the experimental setup with the gold (Au) nanocontact (NC). The Au NC was formed between two Au bases connecting with the quartz length-extension resonator (LER) edge and the counterelectrode, respectively. We observed the Au NC by TEM simultaneously with measuring its electrical conductance and stiffness. The Au NC was formed as shown in the inset. (b) A typical TEM image of the gold [111] nanocontact. The inset shows the structure model viewing from the same direction. (c) Three-dimensional illustration of gold [111] nanocontact. Three {111} facets (hexagonal pattern) are slightly truncated by three {001} facets (square pattern).

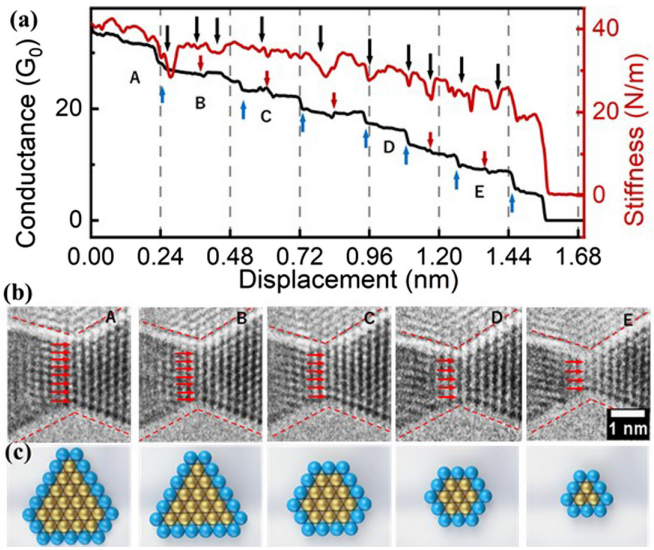

FIG. 2. (a) Typical evolution of electrical conductance and stiffness during stretching the Au nanocontact (NC) with the axis along the ⟨111⟩ direction at a speed of 0.08 nm/s. In the stiffness curve, the black arrows indicate dips, and in the conductance curve, the blue and red arrows indicate stepwise drops and fluctuations, respectively. (b) TEM images taken at the conductance plateaus of A–E in (a), respectively. In TEM images, the red dotted lines are drawn along the outline of the gold nanocontact, indicating that the angles of the apex are always the same (~55°) during stretching. The red arrows indicate the Au atoms at the smallest cross section. (c) The cross-sectional atomic configurations of the narrowest (111) layer at the conductance plateaus of A–E in (a), retrieved from both conductance values and TEM images. The blue and yellow circles correspond to the surface and core atoms, respectively.

was controlled by a tube piezo (fine motion) and an ultrasonic linear motor (TULA50, Technohands, coarse motion). The Au wires were baked in advance at ~100°C for at least 24 h in a vacuum chamber. Afterward, the Au tip surfaces were irradiated with an intense electron beam (beam density: ~100 A/cm^2) in the UHV-TEM to remove the contaminations adsorbed on it. During TEM observation, the electrical conductance was measured by applying the bias voltage of 0.01 V to the NC for estimating its minimum cross-sectional area [40]. Simultaneously, for estimating the mechanical response of the NC, the LER prong oscillated at its resonant frequency with a constant amplitude of 27 pm by application of the ac excitation voltage via a phase-locked loop with an oscillation controller (OC4, SPECS). The stiffness of the Au NC was derived from the shift of the LER resonant frequency [38]. Note that the measured stiffness included not only the contribution of the introduced layer but also contribution of the remaining part (both sides' base including the bulk parts) supporting it. In the previous report [37,39], the Au NC stiffness might be underestimated by tens of percent if the contribution of the bases was not considered. In the present Letter, we precisely determined Young's modulus of the introduced layer by taking the contribution of the bases into account. Figure 1(b) shows a typical TEM image of the Au ⟨111⟩ NC, showing an "hourglass" shape. It was formed between both apexes of two triangular pyramidal tips surrounded by three {111} facets and slightly truncated by three {001} facets as shown in Fig. 1(c), which were consistent with Wulff's theorem [41,42].

Figure 2(a) shows a typical evolution of the measured stiffness and electrical conductance of the Au ⟨111⟩ NC when stretching at a constant speed (see Movie S1 in the Supplemental Material [43]). From TEM observation, a new (111) layer was found to be introduced every ca. 0.24 nm of stretching as reported previously [42]. The stepwise drop (as marked by the blue arrows) in conductance appeared simultaneously with introduction of the (111) layer. It means that the introduced (111) layer had a smaller cross section than the narrowest one before the introduction. When the NC was stretched beyond 0.96 nm, the period of the atomic layer introduction became shorter than 0.24 nm, possibly due to the surface effect of the thin layer introduction. On the other hand, small fluctuations (as marked by the red arrows) sometimes appeared in the conductance plateaus. Because no new introduced layer was observed there, they might be caused by rearrangement or slip of the inserted (111) layers.

From the TEM images of the Au ⟨111⟩ NCs viewed from the [110] direction during the stretching process [Fig. 2(b) A–E], the number of atoms at the width of the narrowest (111) layer was counted to be 8, 7, 6, 5, and 4 atoms, respectively, as indicated by the red arrows in Fig. 2(b). Such observation with measurement of the conductance value invaluably give information about the atomic arrangement of the introduced (111) layer. When the (111) layer was introduced, the other parts were confirmed to be unchanged by the TEM observation, which showed that the apex angle of both pyramidal bases was kept at 55° [Fig. 2(b)], the introduced layer should be made by surface migration of atoms from the bulk parts as discussed later.

On the other hand, the stiffness curve shows some small plateaus separated by some dips. These small plateaus could correspond to the elastic deformation. The dips appeared in response to the drops or fluctuations in conductance, as indicated by the black arrows in the stiffness curve of Fig. 2(a). Previously, such dips have been pointed out to appear in stiffness curve when the target material was plastically deformed [45,46]. It was probable that the stiffness was temporarily reduced due to unstable atomic configurations at the moment of plastic deformation.

The shape of the narrowest (111) layer was identified by combining the TEM image and the electrical conductance. Based on the Sharvin formula [40], the areas of the narrowest cross section in the TEM images from A–E in Fig. 2 were estimated to be approximately 2.7, 2.3, 1.9, 1.4, and 0.8 nm^2, respectively, since the conductance values were measured to be 31.6, 26.7, 22.2, 16.3, and 9.5 G_0 ($=2e^2/h$: the quantized unit of conductance, where e is the elementary charge, and h is the Planck constant), respectively [17]. Assuming that one Au atom in the (111) plane occupies 0.071 nm^2 (detail in the Supplemental Material [43]), the number of atoms in the narrowest layer could be estimated as 38, 33, 27, 19, and 12 atoms, respectively. Considering that such a thin Au ⟨111⟩ NC has a threefold symmetric shape [see Fig. 1(c)] [41,47], the atomic configuration of the narrowest (111) layer was determined to be a triangle or truncated triangle shape that was mainly composed of {111} facets [Fig. 2(c)]. Note that the surface shrinkage can be ignored since it is estimated to be 1%–1.3% even in the narrowest cross section of 7 atoms due to the average coordination number of about 7.8 [48,49].

A model is proposed to calculate the Young's modulus of the inserted atomic layer as shown in Fig. 3(a). The nanocontact can be regarded as a series coupling of atomically thin disks [39]. Thus, the stiffness measured after the introduction of the atomic layer (k_{after}) can be expressed as a series coupling of the stiffness of the introduced layer (k_{layer}) and the stiffness of the two base parts (k_{base}) as

$$\frac{1}{k_{\mathrm{after}}} = \frac{1}{k_{\mathrm{layer}}} + \frac{1}{k_{\mathrm{base}}}. \tag{1}$$

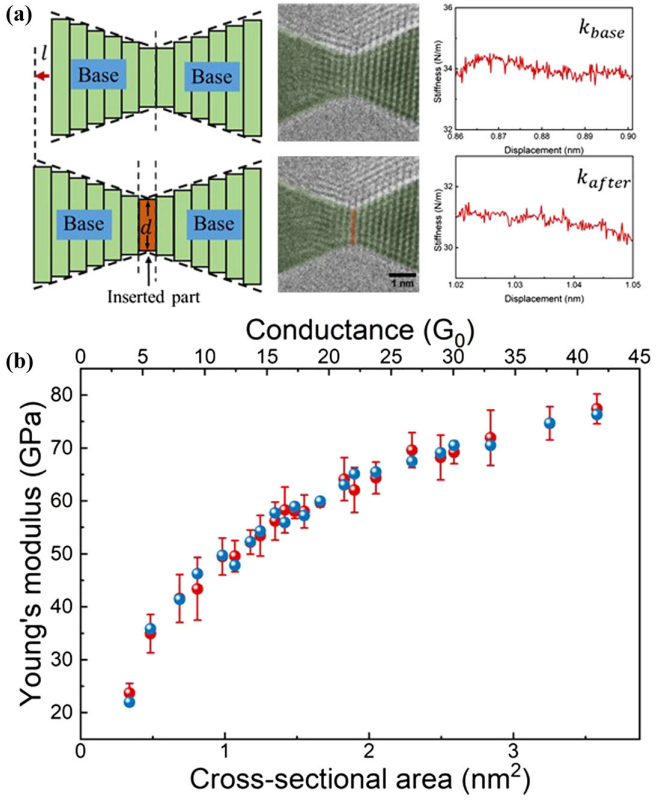

FIG. 3. (a) TEM images and corresponding models and stiffness of the Au ⟨111⟩ NC taken before and after the introduction of a (111) layer. One the (111) layer was introduced as a minimum cross section to keep the apex angle of the pyramidal NC constant. The curves of the corresponding stiffness plateaus, retrieved from Fig. 2(a), were also shown. (b) Young's modulus of the Au ⟨111⟩ NC as a function of the cross-sectional area. The red dots and error bars correspond to the average and standard deviation, respectively. The blue dots correspond to the value obtained by fitting the experimental values with Eq. (3).

Because both sides' base parts were unchanged before and after the introduction of (111) layer, $k_{\mathrm{base}} = k_{\mathrm{before}}$, where the k_{before} is the stiffness measured before the introduction of (111) layer. k_{before} and k_{after} were obtained by averaging the flat plateaus in stiffness curve before and after the introduction of the (111) layer [Fig. 3(a) as an example]. However, the plateau regions could not be always observed both before and after the introduction of the new layer in time evolution of stiffness. The drop or fluctuation in stiffness sometimes did not always match with the introduction of the new layer. In such cases, the stiffness of the new layer could not be estimated.

From Hook's law, the Young's modulus of the inserted layer (Y_{layer}) can be obtained as

$$Y_{\mathrm{layer}} = \frac{F/A}{\Delta l/l} = \frac{k_{\mathrm{layer}} l}{A} = \frac{k_{\mathrm{before}} k_{\mathrm{after}}}{k_{\mathrm{before}} - k_{\mathrm{after}}} \times \frac{l}{A}, \tag{2}$$

where l is the layer thickness, corresponding to the spacing between the (111) planes in Au lattice (ca. 0.24 nm), and A

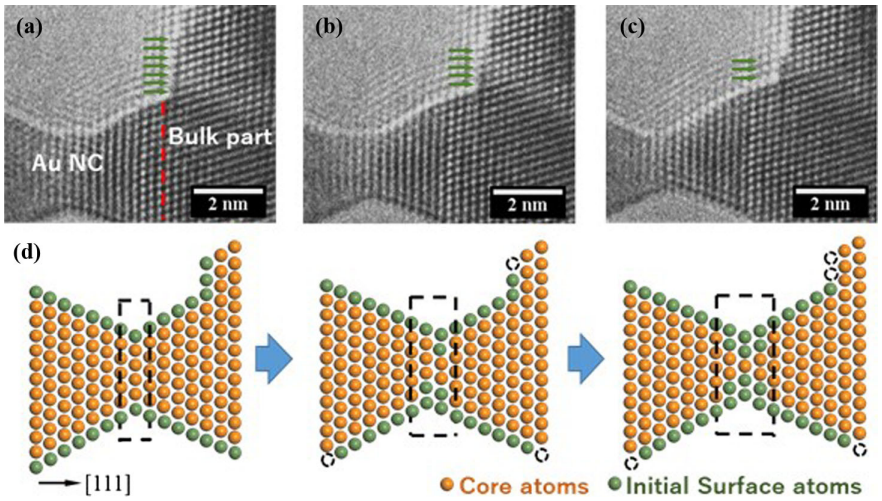

FIG. 4. (a)–(c) A series of TEM images of the bulk part supporting the Au ⟨111⟩ NC during stretching. The number of the surface atoms indicated by green arrows decreased one-by-one, indicating migration of these atoms on the surface. The dashed red line indicates the boundary between the bulk part and the Au NC. The lattices were observed to be slightly distorted in the pyramidal shape; such distortion could be caused by slight deviation of the stretching direction from the [111] orientation (the axis of the NC). (d) Schematic illustration of introduction of a (111) layer to the minimum cross section of the Au NC due to migration of surface atoms. The dashed circles indicate the original positions of the migrated surface atoms. The dashed boxes indicate the deformation region.

is the cross-sectional area, which is determined as shown in Fig. 2(c).

We statistically analyzed 28 stretching curves to obtain the dependence of Young's modulus on the cross-sectional area [Fig. 3(b)], showing that the Young's modulus gradually decreases with decreasing size (detail in supporting information). Young's modulus was estimated to be approximately 80 GPa when the cross-sectional area was about 3.6 nm^2 (corresponding to the diameter of about 2.1 nm). It decreased to about 30 GPa at the cross-sectional area of ca. 0.35 nm^2 (corresponding to the diameter of about 0.7 nm). The estimated Young's modulus was remarkably smaller than the theoretical one of ca. 116 GPa, which was supposed to correspond to the value under stretching bulk Au crystal along the [111] direction [50]. In such small size (below a few nm in size), since the surface-to-volume ratio has been pointed out not to be ignored, the surface effect was thought to play an important role in determining the Young's modulus [51,52].

As concerned with the surface effect, Young's modulus of the metal NWs has been quantitatively analyzed through core-shell models [13,53] and core-surface models [51,52,54]. Assuming that the core is surrounded by the surface atomic layer with a different Young's modulus, the Young's modulus of the introduced layer (Y_{layer}) can be obtained by summation of weighted Young's modulus of core (Y_{core}) and surface (Y_{surface}) as:

$$Y_{\mathrm{layer}} = Y_{\mathrm{surface}} \frac{A_{\mathrm{surface}}}{A_{\mathrm{layer}}} + Y_{\mathrm{core}} \frac{A_{\mathrm{core}}}{A_{\mathrm{layer}}}, \tag{3}$$

where A_{surface} and A_{core} are the numbers of the surface atoms and the core atoms in the introduced layer, respectively. From the atomic configurations in the introduced (111) layer estimated as shown in Fig. 2(c), the number of the surface atoms and the core atoms was determined, where the surface atoms were defined as those in the outermost layer denoted by the blue spheres and the core atoms were denoted by the yellow spheres.

By fitting equation (3) to the experimental data of Fig. 3(b) using the Levenberg-Marquardt method [55], Young's moduli of the surface and core atoms were retrieved to be 22 and 119 GPa, respectively, with a coefficient of determination of 91.4%. The obtained Young's modulus of the core part was close to that of the bulk [111] crystal (116 GPa), while the one of the surface was much lower than that of the core. It implies that the outermost surface has unique mechanical properties and plays an important role in determination of overall mechanical properties of sub-two-nm Au nanomaterials. Assuming that the outermost surface, subsurface, and core had different Young's moduli, the subsurface Young's modulus was obtained to be close to the core one, indicating that the model consisting of the outermost surface and core was more suitable for explaining the experimental results. This means that the interatomic potential at the surface is a more gradual slope than one at the core. The interatomic potential at the surface, which is mainly governed by their low coordination number, could be evaluated through further structural and force analysis by our method that paves the way for understanding the physical properties of nanomaterials whose surface effect cannot be ignored.

It is reasonable that the surface Young's modulus was quite low because the surface atoms were observed to be easily diffused, which were weakly bonded with the

subsurface. As shown in Figs. 4(a) and S5, and videos S2 and S3 in the Supplemental Material [45], the surface atoms located on a side of the Au bulk part disappeared one by one during stretching of the Au ⟨111⟩ NCs. It means that these surface atoms migrated to the narrowest part of the NC. These atoms seemed to migrate more frequently on the (111) surface as shown in the supporting videos [43]. Such surface diffusion governing deformation process was pointed out to explain the reshaping of Au nanorods below melting temperatures but was not experimentally clarified [56,57]. Therefore, the plastic deformation of the Au ⟨111⟩ NC are thought to be different from conventional brittle or ductile fracture of bulk Au crystal as shown in Fig. 4(d). When a Au ⟨111⟩ NC is plastically deformed, the surface atoms migrating on the NC are incorporated in introduction of a (111) layer while the other parts are unchanged.

In conclusion, we measured the stiffness evolution of a clean Au ⟨111⟩ NC with a diameter below 2 nm simultaneously with observation of the structure and measurement of the electrical conductance using our developed TEM holder equipped with a quartz LER. We observed that a single (111) layer was introduced at the minimum cross section of the NC each time when stretching by 0.24 nm. By analyzing the stretching process, Young's modulus of the Au ⟨111⟩ NC was estimated to gradually decrease from 80 to 30 GPa as the diameter decreased below 2 nm. This size dependence was well explained by a model of the surface with a low surface Young's modulus of 22 GPa. This study demonstrated the clarification of the surface effect on mechanical response for the nanocontacts, which indicates that the surface is softened due to low coordination number.

This work was supported by JSPS KAKENHI (Grants No. 18H01825 and No. 18H03879). J. Z. acknowledges financial support by the Sasakawa Scientific Research Grant from The Japan Science Society and the Exchange Research Grant Project from Marubun Research Promotion Foundation.

*Corresponding author.
oshima@jaist.ac.jp

[1] E. P. M. Amorim and E. Z. da Silva, Helical Gold Nanowires Make Longer Linear Atomic Chains, Phys. Rev. Lett. **101**, 125502 (2008).
[2] Q. F. Gu, G. Krauss, F. Gramm, A. Cervellino, and W. Steurer, Unexpected High Stiffness of Ag and Au Nanoparticles, Phys. Rev. Lett. **100**, 045502 (2008).
[3] M. Lebrat, S. Häusler, P. Fabritius, D. Husmann, L. Corman, and T. Esslinger, Quantized Conductance through a Spin-Selective Atomic Point Contact, Phys. Rev. Lett. **123**, 193605 (2019).
[4] H. Ohnishi, Y. Kondo, and K. Takayanagi, Quantized conductance through individual rows of suspended gold atoms, Nature (London) **395**, 780 (1998).
[5] Y. Oshima, A. Onga, and K. Takayanagi, Helical Gold Nanotube Synthesized at 150 K, Phys. Rev. Lett. **91**, 205503 (2003).
[6] Y. Kondo and K. Takayanagi, Synthesis and characterization of helical multi-shell gold nanowires, Science **289**, 606 (2000).
[7] Y. Oshima, H. Koizumi, K. Mouri, H. Hirayama, K. Takayanagi, and Y. Kondo, Evidence of a single-wall platinum nanotube, Phys. Rev. B **65**, 121401(R) (2002).
[8] Y. Yao and S. Chen, Surface effect in the bending of nanowires, Mech. Mater. **100**, 12 (2016).
[9] T. Y. Zhang, Z. J. Wang, and W. K. Chan, Eigenstress model for surface stress of solids, Phys. Rev. B **81**, 195427 (2010).
[10] M. J. Lagos, F. Sato, D. S. Galvão, and D. Ugarte, Mechanical Deformation of Nanoscale Metal Rods: When Size and Shape Matter, Phys. Rev. Lett. **106**, 055501 (2011).
[11] S. D. Bennett, J. Maassen, and A. A. Clerk, Scattering Approach to Backaction in Coherent Nanoelectromechanical Systems, Phys. Rev. Lett. **105**, 217206 (2010).
[12] X. Li, T. Ono, Y. Wang, and M. Esashi, Ultrathin single-crystalline-silicon cantilever resonators: Fabrication technology and significant specimen size effect on Young's modulus, Appl. Phys. Lett. **83**, 3081 (2003).
[13] C. Q. Chen, Y. Shi, Y. S. Zhang, J. Zhu, and Y. J. Yan, Size Dependence of Young's Modulus in ZnO Nanowires, Phys. Rev. Lett. **96**, 075505 (2006).
[14] A. Sánchez-Iglesias, B. Rivas-Murias, M. Grzelczak, J. Pérez-Juste, L. M. Liz-Marzán, F. Rivadulla, and M. A. Correa-Duarte, Highly transparent and conductive films of densely aligned ultrathin Au nanowire monolayers, Nano Lett. **12**, 6066 (2012).
[15] S. Gong, W. Schwalb, Y. Wang, Y. Chen, Y. Tang, J. Si, B. Shirinzadeh, and W. Cheng, A wearable and highly sensitive pressure sensor with ultrathin gold nanowires, Nat. Commun. **5**, 3132 (2014).
[16] L. G. Zhou and H. Huang, Are surfaces elastically softer or stiffer?, Appl. Phys. Lett. **84**, 1940 (2004).
[17] R. E. Miller and V. B. Shenoy, Size-dependent elastic properties of nanosized structural elements, Nanotechnology **11**, 139 (2000).
[18] S. J. A. Koh and H. P. Lee, Molecular dynamics simulation of size and strain rate dependent mechanical response of FCC metallic nanowires, Nanotechnology **17**, 3451 (2006).
[19] G. Wang and X. Li, Predicting Young's modulus of nanowires from first-principles calculations on their surface and bulk materials, J. Appl. Phys. **104**, 113517 (2008).
[20] S. Liu, W. Y. Wen, and Z. Zhu, The elastic properties and energy characteristics of Au nanowires: An atomistic simulation study, Chin. Phys. B **17**, 2621 (2008).
[21] Z. J. Wang, C. Liu, Z. Li, and T. Y. Zhang, Size-dependent elastic properties of Au nanowires under bending and tension—surfaces versus core nonlinearity, J. Appl. Phys. **108**, 083506 (2010).
[22] M. D. Uchic, D. M. Dimiduk, J. N. Florando, and W. D. Nix, Sample dimensions influence strength and crystal plasticity, Science **305**, 986 (2004).
[23] J. H. Seo, Y. Yoo, N. Y. Park, S. W. Yoon, H. Lee, S. Han, S. W. Lee, T. Y. Seong, S. C. Lee, K. B. Lee, P. R. Cha,

H. S. Park, B. Kim, and J. P. Ahn, Superplastic deformation of defect-free Au nanowires via coherent twin propagation, Nano Lett. **11**, 3499 (2011).
[24] K. Gall, J. Diao, and M. L. Dunn, The strength of gold nanowires, Nano Lett. **4**, 2431 (2004).
[25] J. Diao, K. Gall, and M. L. Dunn, Atomistic simulation of the structure and elastic properties of gold nanowires, J. Mech. Phys. Solids **52**, 1935 (2004).
[26] S. Sun, D. Kong, D. Li, X. Liao, D. Liu, S. Mao, Z. Zhang, L. Wang, and X. Han, Atomistic mechanism of stress-induced combined slip and diffusion in sub-5 nanometer-sized Ag nanowires, ACS Nano **13**, 8708 (2019).
[27] J. Wang, F. Sansoz, J. Huang, Y. Liu, S. Sun, Z. Zhang, and S. X. Mao, Near-ideal theoretical strength in gold nanowires containing angstrom scale twins, Nat. Commun. **4**, 1742 (2013).
[28] J. Wang, Z. Zeng, C. R. Weinberger, Z. Zhang, T. Zhu, and S. X. Mao, In situ atomic-scale observation of twinning-dominated deformation in nanoscale body-centred cubic tungsten, Nat. Mater. **14**, 594 (2015).
[29] Y. Chen, T. Burgess, X. An, Y. Mai, H. H. Tan, J. Zhou, S. P. Ringer, C. Jagadish, and X. Liao, Effect of a high density of stacking faults on the Young's modulus of GaAs nanowires, Nano Lett. **16**, 1911 (2016).
[30] G. Y. Jing, H. L. Duan, X. M. Sun, Z. S. Zhang, J. Xu, Y. D. Li, J. X. Wang, and D. P. Yu, Surface effects on elastic properties of silver nanowires: Contact atomic-force microscopy, Phys. Rev. B **73**, 235409 (2006).
[31] Y. Wang, L. Wang, H. J. Joyce, Q. Gao, X. Liao, Y. Mai, H. H. Tan, J. Zou, S. P. Ringer, H. Gao, and C. Jagadish, Super deformability and Young's modulus of GaAs nanowires, Adv. Mater. **23**, 1356 (2011).
[32] M. J. Gordon, T. Baron, F. Dhalluin, P. Gentile, and P. Ferret, Size effects in mechanical deformation and fracture of cantilevered silicon nanowires, Nano Lett. **9**, 525 (2009).
[33] Y. Zhu, F. Xu, Q. Qin, W. Y. Fung, and W. Liu, Mechanical properties of vapor–liquid–solid synthesized silicon nanowires, Nano Lett. **9**, 3934 (2009).
[34] Y. Chen, Q. Gao, Y. Wang, X. An, X. Liao, Y. Mai, H. H. Tan, J. Zou, S. P. Ringer, and C. Jagadish, Determination of Young's modulus of ultrathin nanomaterials, Nano Lett. **15**, 5279 (2015).
[35] P. Jelínek, R. Pérez, J. Ortega, and F. Flores, Ab initio study of evolution of mechanical and transport properties of clean and contaminated Au nanowires along the deformation path, Phys. Rev. B **77**, 115447 (2008).
[36] B. Wu, A. Heidelberg, and J. J. Boland, Mechanical properties of ultrahigh-strength gold nanowires, Nat. Mater. **4**, 525 (2005).
[37] J. Zhang, K. Ishizuka, M. Tomitori, T. Arai, K. Hongo, R Maezono, E. Tosatti, and Y. Oshima, Peculiar atomic bond nature in platinum monatomic chains, Nano Lett. **21**, 3922 (2021).
[38] J. Zhang, K. Ishizuka, M. Tomitori, T. Arai, and Y. Oshima, Atomic scale mechanics explored by in situ transmission electron microscopy with a quartz length-extension resonator as a force sensor, Nanotechnology **31**, 205706 (2020).
[39] K. Ishizuka, M. Tomitori, T. Arai, and Y. Oshima, Mechanical analysis of gold nanocontacts during stretching using an in-situ transmission electron microscope equipped with a force sensor, Appl. Phys. Express **13**, 025001 (2020).
[40] Y. V. Sharvin, A possible method for studying Fermi surfaces, Eksp. Teor. Fiz. **48**, 2 (1965), http://jetp.ras.ru/cgi-bin/dn/e_021_03_0655.pdf.
[41] Y. Oshima, K. Mouri, H. Hirayama, and K. Takayanagi, Development of a miniature STM holder for study of electronic conductance of metal nanowires in UHV–TEM, Surf. Sci. **531**, 209 (2003).
[42] Y. Oshima, Y. Kurui, and K. Takayanagi, One-by-one introduction of single lattice planes in a bottlenecked gold contact during stretching, J. Phys. Soc. Jpn. **79**, 054702 (2010).
[43] See Supplemental Material at http://link.aps.org/supplemental/10.1103/PhysRevLett.128.146101 for further information on the experimental details and analysis procedures, which includes Ref. [44].
[44] W. P. Davey, Precision measurements of the lattice constants of twelve common metals, Phys. Rev. **25**, 753 (1925).
[45] J. Comtet, A. Lainé, A. Niguès, L. Bocquet, and A. Siria, Atomic rheology of gold nanojunctions, Nature (London) **569**, 393 (2019).
[46] T. Shiota, A. I. Mares, A. M. C. Valkering, T. H. Oosterkamp, and J. M. van Ruitenbeek, Mechanical properties of Pt monatomic chains, Phys. Rev. B **77**, 125411 (2008).
[47] Y. Kurui, Y. Oshima, M. Okamoto, and K. Takayanagi, Conductance quantization and dequantization in gold nanowires due to multiple reflection at the interface, Phys. Rev. B **79**, 165414 (2009).
[48] J. T. Steven, V. B. Golovko, B. Johannessen, and A. T. Marshall, Electrochemical stability of carbon-supported gold nanoparticles in acidic electrolyte during cyclic voltammetry, Electrochim. Acta **187**, 593 (2016).
[49] J. T. Miller, A. J. Kropf, Y. Zha, J. R. Regalbuto, L. Delannoy, C. Louis, E. Bus, and J. A. van Bokhoven, The effect of gold particle size on Au–Au bond length and reactivity toward oxygen in supported catalysts, J. Catal. **240**, 222 (2006).
[50] H. Petrova, J. Perez-Juste, Z. Zhang, J. Zhang, T. Kosel, and G. V. Hartland, Crystal structure dependence of the elastic constants of gold nanorods, J. Mater. Chem. **16**, 3957 (2006).
[51] J. Zhang, Small-scale effect on the piezoelectric potential of gallium nitride nanowires, Appl. Phys. Lett. **104**, 253110 (2014).
[52] H. Lu and X. Meng, Correlation between band gap, dielectric constant, Young's modulus and melting temperature of GaN nanocrystals and their size and shape dependences, Sci. Rep. **5**, 16939 (2015).
[53] F. Xu, Q. Qin, A. Mishra, Y. Gu, and Y. Zhu, Mechanical properties of ZnO nanowires under different loading modes, Nano Res. **3**, 271 (2010).
[54] R. C. Cammarata, Surface and interface stress effects in thin films, Prog. Surf. Sci. **46**, 1 (1994).
[55] C. Kanzow, N. Yamashita, and M. Fukushima, Levenberg–Marquardt methods with strong local convergence properties for solving nonlinear equations with convex constraints, J. Comput. Appl. Math. **172**, 375 (2004).

[56] W. J. Kennedy, S. Izor, B. D. Anderson, G. Frank, V. Varshney, and G. J. Ehlert, Thermal reshaping dynamics of gold nanorods: Influence of size, shape, and local environment, ACS Appl. Mater. Interfaces **10**, 43865 (2018).

[57] A. B. Taylor, A. M. Siddiquee, and J. W. M. Chon, Below melting point photothermal reshaping of single gold nanorods driven by surface diffusion, ACS Nano **8**, 12071 (2014).